Numerical simulation of cyclic oxidation kinetics with automatic fitting of experimental data

S. Sureau, D. Poquillon and D. Monceau

CIRIMAT, ENSIACET, 118 Route de NArbonne, 31077 Toulouse, France

This paper proposes a model, based on a Monte Carlo method, to assess cyclic oxidation tests. The numerical code fits automatically the experimental net mass change curves. Oxidation kinetics are identified as well as the relationship between spalling and local oxide thickness or time. The modelling is applied to cyclic oxidation of NiPtAl single crystals at 1150 °C in dry air.

Keywords: Nickel aluminides; Oxidation; Kinetics; Monte Carlo techniques

Some components of gas turbines are submitted to corrosion, oxidation and mechanical stresses in the temperature range of 700–1200 °C. This study focuses on degradation due to cyclic oxidation. Materials designed to be used in these conditions develop a protective oxide layer which prevents rapid oxidation and material failure. However, during thermal cycling, thermal expansion mismatch between the oxide scale and the alloy induces stresses which add to growth stresses and lead to oxide spallation. To study this degradation in the laboratory, gravimetry can be used to assess the oxidation and spallation behaviour of materials [1], [2] and [3]. Several models have been used to assess cyclic oxidation kinetics [4], [5], [6], [7], [8], [9], [10] and [11]. In Refs. [4], [6] and [11], the surface is divided into independent cells. Oxide growth and spalling are deterministic as in the original two-parameter Smialek model [4], in some COSP models [5], in the p-kp model [10] and in the DICOSM model [11]. In the COSP model [5] and [12], a Monte Carlo option is also available, which treats the spalling of each cell of the surface as resulting from a given probability function. In Strehl's model [9], the surface is divided into regular hexagonal cells and the influence of the neighbouring cells on the probability of spallation of cells around the spalled area can be studied. The present work presents a program which automatically fits experimental net mass change curves in order to quantify the oxidation kinetics. Oxidation kinetics and oxide spalling are modelled with a Monte Carlo approach. Several laws for the oxidation kinetics and the relationship between spallation and the local oxide thickness are tested. The results of the simulations are compared with new experimental data for cyclic oxidation of NiPtAl single crystals at 1150 °C.

NiPtAl (40 at.% Ni, 10 at.% Pt, 50 at.% Al and 90 ppm wt. S) single crystal discs (8 mm diameter and 2 mm thick) were submitted to cyclic and isothermal oxidation tests. The cyclic oxidation tests were performed using a horizontal tube furnace, with synthetic air flowing throughout the whole experiment. The specimens, hanging on a Pt/Rh wire, were inserted into the hot furnace and then removed to a cold chamber where their temperature decreased to 115 °C. The samples were oxidized for 1800 cycles of 1 h at 1150 °C and 15 min in the cold chamber. The net mass change (NMC) was followed as function of cycle number using a Sartorius Genius^{TM} microbalance with 10 μg accuracy. Isothermal oxidation tests were performed using a Setaram TAG24S under flowing synthetic air throughout the whole experiment. For all tests, samples were hung directly in the gas flow and spalled oxide was not weighed, the heating and cooling rates were 1 °C s^{-1} and the mass variation was continuously measured with an accuracy of 1 μg.

Isothermal tests at 20 and 100 h were performed at 1150 °C, in order to determine the oxidation kinetics and to validate the image analysis procedure developed to quantify spallation for the cyclic test.

Samples were observed using a LEO435 scanning electron microscope (SEM). In order to limit delayed or desktop spallation, which would affect quantification of the spalled area. The samples were observed the day they were removed from the furnace. The samples were observed with backscattered electrons every 126 cycles. The acceleration voltage was 15 kV, the probe current 2 nA and the working distance 15 mm. The magnification was sufficient to see all the spalled areas and to cover the whole surface of the sample with four images in order to perform a statistical approach (1 pixel for $4 \times 4\ \mu m^2$). Furthermore, using backscattered electrons enhanced the differences between the zones with different oxide scale thickness (Fig. 1(a)). The image analysis software Scion Image^{TM} was used to quantify the proportion of surface where oxide scale had spalled. A method has been developed to compare the results obtained at various stages of cyclic oxidation. Using the histogram of the distribution of the 256 greyscale SEM images (Fig. 1(a)), a threshold was determined in order to separate freshly spalled areas from reoxidized areas. A binary image was then generated. On the reversed binary picture (Fig. 1(b)), the spalled areas appear in black. Zones with a size smaller than 1 pixel were removed as they do not correspond to spalled areas (noise reduction). On the corresponding binary image, the proportion of spalled area was automatically calculated. These operations were carried out on all the images of the sample after different numbers of cycles.

Figure 1. NiPtAl after 1674 cycles: (a) SEM picture (256 grey levels), (b) corresponding reversed binary picture.

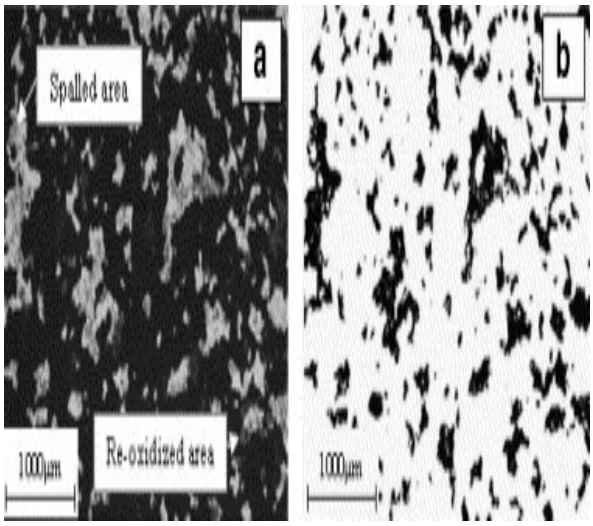

Oxide scales formed during oxidation were also analysed by X-ray diffraction (XRD) with a Seifert XRD 3000 TT diffractometer using a 5° grazing incidence.

One sample of NiPtAl was oxidized in the thermobalance with a heating rate of 1 °C min^{-1}, followed by 20 h at 1150 °C and then cooled down at an initial cooling rate of 1 °C min^{-1}. This experiment allowed quantitative evaluation of the percentage of the scale which spalled during cooling, for a known oxide scale thickness. With the symmetrical furnace arrangement of the

thermobalance used for this study, the effect of buoyancy on mass was limited but could not be neglected. A careful analysis of the continuous mass recording during heating, dwell and cooling showed that 0.014 mg cm^{-2} of oxygen was gained during heating, followed by 0.302 mg cm^{-2} during the 20 h dwell. This corresponds to an overall mass gain of 0.316 mg cm^{-2} of oxygen, i.e. 0.671 mg cm^{-2} of oxide, corresponding to an oxide scale thickness of 1.7 μm. During cooling a mass loss due to spalling of 0.017 mg cm^{-2} was measured after correcting for the buoyancy effect. This value corresponds to 2.5% of the oxide scale. On the same sample, the spallation area was determined by image analysis and a value of 3.0% was found.

Another NiPtAl sample was oxidized isothermally for 100 h at 1150 °C (isothermal). Using the local parabolic fitting method [13] on the last 50 h of the test, we can determine the parabolic oxidation kinetics coefficient (k_p) at 1150 °C. We obtained a k_p of 1.8×10^{-6} mg^2 cm^{-4} s^{-1}. This value will be used for some of our cyclic oxidation kinetics simulations.

A third NiPtAl sample was oxidized for 1800 cycles of 1 h at 1150 °C. The NMC variation (black symbols on Fig. 2(a)) shows the classical shape of cyclic oxidation curves due to a combination of oxidation and spallation. The steady-state stage (linear decrease of mass) was reached after about 1000 cycles. During the steady-state, the increase of mass due to oxidation equals the mass of oxide lost by spalling at each cycle. XRD analysis after 1800 cycles revealed that the oxide scale is composed of α-Al_2O_3. The experimental evolution of spalling as a function of the number of cycles is plotted in Figure 2(b) (black marks). After 126 cycles, the spalling area represents 0.1% of the surface and this proportion increases rapidly for 1000 cycles, after which it is difficult to state if it stabilizes around 2–5% or continues to increase. This stage corresponds to an average oxide thickness of about 4.6 μm. This last value was measured on a cross section of the specimen observed by SEM.

Figure 2. NiPtAl (S = 90 ppm wt.) oxidized 1800 × 1 h at 1150 °C in synthetic air: (a) NMC curve and (b) spalling area. Black marks: experimental data, simulations 1 and 3: $k_p = 1.8 \times 10^{-6}$ mg^{-2} cm^{-4} s^{-1} and simulation 1: p_{max} = 3%, simulation 3: p_{max} = 1.2%, simulation 2: experimental isothermal mass gain data and p_{max} = 3%.

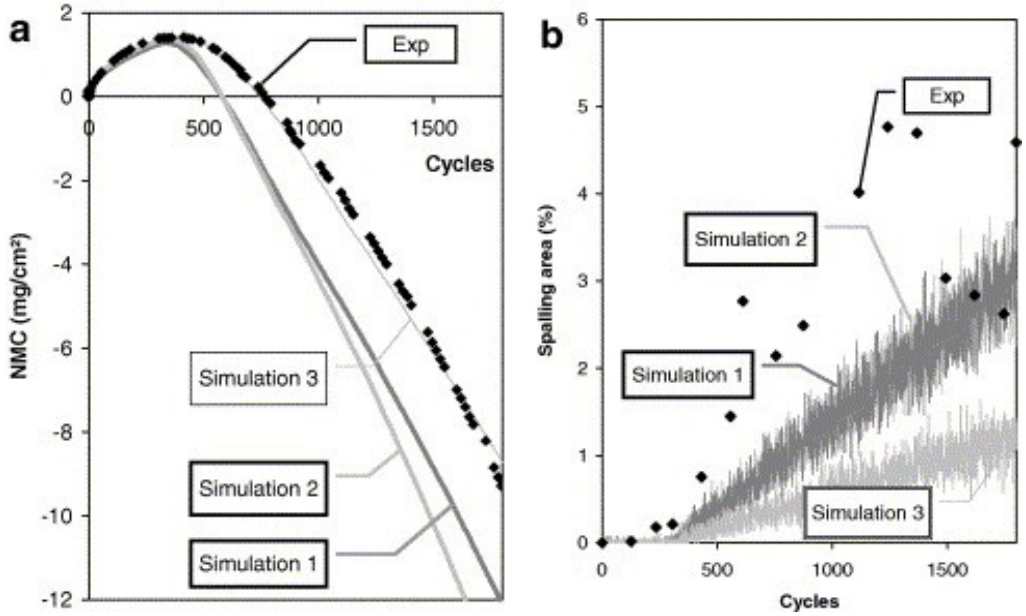

An automatic program was developed to fit a cyclic oxidation model to experimental data. Cyclic oxidation modelling follows a statistical approach based on a Monte Carlo simulation. This model is based on the hypotheses that (i) oxidation kinetics during high-temperature dwell is parabolic and the oxidation kinetics, k_p, is the same for all the cycles; (ii) spallation occurs at the metal/oxide interface; and (iii) oxidation occurring during heating and cooling can be neglected compared to oxidation during high-temperature dwell.

The surface is divided into 2800 independent cells. Each of the cells has a probability $p_j(e)$ of spallation. For each cell, a random number is generated (Monte Carlo approach) between 0 and 1. If this value is below $p_j(e)$, the cell spalls. Oxidation kinetics (k_p) is linked to the local oxide thickness e_j on the cell j, to the mass of oxygen per unit volume of oxide mOx, and to the cumulative oxidation duration t_j since the last spalling on the particular cell j by:

$$k_p = \frac{(mOx \cdot e_j)^2}{t_j}. \quad (1)$$

Different spalling probability laws were tested. The first series of tests were done with a spalling probability p_j which depends on the local oxide thickness (Fig. 3):

$$p_j = \alpha \cdot \left(\frac{e_j}{e_{max}}\right)^i \text{ with } \quad e_{max} = \frac{\sqrt{k_p \cdot t}}{mOx}, \quad (2)$$

where i is an integer in the range [0–4] describing the dependence of spalling probability on the local oxide thickness, α is a constant to be determined ($0 < \alpha < 1$) and t is the cumulative oxidation duration. It should be noted that Eq. (3) implies that the spalling probability p is always less than 1. During the automatic fitting of a NMC curve, the different values of i are tested successively using the minimization algorithm of the error function:

$$F = \sum_{n=n_0}^{n_f} (n^4 \cdot (\mathrm{NMG}_{\mathrm{exp}} - \mathrm{NMG}_{\mathrm{num}})^2), \tag{3}$$

where n_0 and n_f are respectively the number of the first and last cycles. This function emphasizes the influence of the final points of the experimental curve. The increase of p with the local oxide scale thickness is justified by the higher level of stress in a thicker oxide scale during cooling [14] and [15]. This increase of spalling with oxide scale thickness has been used in several previous models [5] and [6].

Figure 3. NiPtAl (S = 90 ppm wt.) oxidized 1800 × 1 h at 1150 °C in synthetic air.

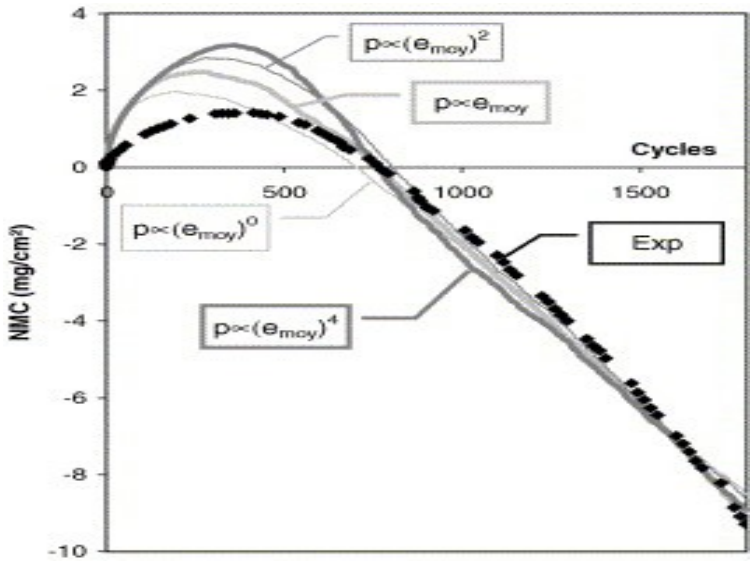

In the second series of tests, the spalling probability is independent of the local oxide thickness but is time dependent (Fig. 2). This behaviour is expected if the physical or chemical nature of the metal/oxide interface is changing with time. In the case of NiAl aluminide oxidation, cavity nucleation and growth, decrease of Al concentration, increase of S segregation, and β–γ phase transformation at the metal/oxide interface could occur and lead to an increase of spalling with time.

The influence of the local oxide thickness on the cyclic oxidation kinetics was tested using the simulations reported in Figure 3 and Table 1.

Table 1.

Results of the numerical simulation with p as a function of e

I	**0**	**1**	**2**	**4**
k_p (mg^2 cm^{-4} s^{-1})	1.23×10^{-5}	1.23×10^{-5}	1.18×10^{-5}	1.08×10^{-5}

I	0	1	2	4
$p = f(e)$	1.7×10^{-3}	$7.37 \times 10^{-1} e$	$2.91 \times 10^{2} e^{2}$	$6.02 \times 10^{7} e^{4}$
Average oxide thickness after 1800 cycles (μm)	23.9	21.7	20.9	18.8
p at cycle 1800	1.7×10^{-3}	1.6×10^{-3}	1.37×10^{-3}	7.52×10^{-4}

Numerical calculations show that for all simulations, the distribution of local oxide scale thicknesses and the average oxide thickness, e_{av}, become constant after 500 cycles. The final values of $p(e)$ and e_{av} are reported in Table 1. The fitted values of k_p are found to be almost one order of magnitude higher than the isothermal k_p value for the same material (1.8×10^{-6} mg^2 cm^{-4} s^{-1}). The oxide scale thicknesses (18–24 μm) are also much higher than the experimental value (4.6 μm). Another finding is that the effect of the dependence of p on the oxide thickness does not greatly affect the ability of the model to fit the experimental data during the stationary state (linear decrease of the NMC curve in Fig. 3). Indeed, during this regime, the oxide scale thickness distribution is constant and so the average spalling probability is constant too.

Because the calculated average oxide scale thickness and the final spalling parameter, p, were not sufficiently consistent with experimental data, a second set of calculations was performed with a spalling function $p(t)$ increasing with time after a critical number of cycles had been reached. The results are reported in Figure 2 and Table 2. Figure 2(a) compares the three kinetic simulations tested. In simulations 1 and 3, the k_p value determined experimentally is used in the numerical calculation, whereas simulation 2 uses the experimental isothermal mass gain data in order to take into account the transient stage of faster kinetics. Concerning the spalling function (Fig. 2(b)), simulations 1 and 2 used an increasing value up to 3%, which is consistent with the observation of spalled surfaces, whereas simulation 3 used the maximum value of spalling, which allows the best fit of the experimental NMC cyclic oxidation curve.

Table 2.

Results of the numerical simulation with p as a function of time

Simulation	**1**	**2**	**3**
k_p (mg^2 cm^{-4} s^{-1})	1.8×10^{-6}	Isothermal data	1.8×10^{-6}
Average oxide thickness after cycle 1800 (μm)	2.1	1.7	3.5
p at cycle 1800	3%	3%	1.2%

With this second set of simulations (Fig. 2), we can see that the first 300 cycles of the NMC curve are well fitted, contrary to what was observed with the first set of simulations (Fig. 3). The second observation is that taking into account the transient stage during the isothermal oxidation kinetics (simulation 2) does not improve the result. Also, using spalling values close to experimental data (simulations 1 and 2) does not give a correct fit with the experimental NMC curve (Fig. 2(a)).

With this second set of simulations, the calculated average oxide thickness after 1800 cycles (Table 2) is much closer to the experimental value than with the first set of simulations (Table 1). Finally, a better fit is obtained with simulation 3, using the parabolic constant determined experimentally during the isothermal oxidation test, and a spalling function, p, which increases linearly with time after 300 cycles, up to a value of 1.2%, which is lower than the experimental

value (2–5%). The difference between the calculated and observed values could be due to some desktop spalling, as observed originally in Ref. [4] and attributed to the effect of moisture, or due to spalling when samples must be taken out the furnace and the controlled atmosphere to be weighed and handled for the SEM analysis. The calculated average oxide scale thickness is slightly lower than, but in agreement with, the experimental one (3.5 μm instead of 4.6 μm).

A new numerical tool has been developed to assess cyclic oxidation kinetics data via an automatic fitting procedure. This model is based on a Monte Carlo approach and takes into account the increase in spalling probability with local oxide scale thickness or with time. Several kinetics models were tested to reproduce the experimental net mass change during cyclic oxidation of NiPtAl single crystals at 1150 °C in dry air. The average oxide scale thickness was systematically calculated as an output of the simulation and the model gives a useful and independent comparison with experimental data, as well as the extent of spalling determined by image analysis. This work shows that for this specific material, increasing the spalling probability with oxide scale thickness does not improve the fit of the NMC curve since the average oxide scale thickness becomes constant during the final linear stage. In order to obtain an average oxide scale thickness, a final spalling fraction, p, and a parabolic rate constant, k_p, close to the experimental values, the best fit was obtained with a spalling probability increasing with time after a critical number of cycles. This increase of p with time could be linked to an accumulation of damage at the metal/oxide interface (porosities) or to a change of the interfacial chemistry (e.g. the S and Al contents).

This study was partly funded by the French Research Ministry (MENRT Ph.D. grant). The samples were provided by ONERA.

References

M. Schuetze, *Oxid. Met.* **44** (1995), p. 29.

J.L. Smialek, J.A. Nesbitt, C.A. Barrett, C.E. Lowell, in: M. Schuetze, W.J. Quadakkers (Eds.), Cyclic Oxidation of High-Temperature Materials, vol. EFC 27, IOM Communications, London, 1999, p. 148.

European Program COTEST. Test method for thermal cycling oxidation testing at elevated temperatures for metallic materials. RTD Project No. GRD1-2001-40037 M-T, 2005.

J.L. Smialek, *Metall. Trans. A* **9** (1978), p. 309.

C.A. Lowell, J.L. Smialek, C.A. Barrett, in: NACE 6 High-temperature Corrosion, Houston, TX, 1983, p. 219.

C.E. Lowell, C.A. Barrett, R.W. Palmer, J.V. Auping and H.B. Probst, *Oxid. Met.* **36** (1991), p. 81.

K.S. Chan, *Metall. Trans. A* **28** (1997), p. 411.

J.R. Nicholls, R. Newton, M.J. Bennett, H.E. Evans, H. Al-Badairy, G.J. Tatlock, D. Naumenko, W.J. Quadakkers, G. Strehl and G. Borchardt In: M. Schuetze, W.J. Quadakkers and J.R. Nicholls, Editors, *Lifetime Modelling of High-Temperature Corrosion Processes* **EFC 34**, Maney, London (2001), p. 83.

G. Strehl, Ph.D. Thesis, Technischen Universität Clausthal, 2002, p. 132.

D. Poquillon and D. Monceau, *Oxid. Met.* **59** (2003), p. 409.

J.L. Smialek, *Acta Mater.* **51** (2003), p. 469.

J.L. Smialek and J.V. Auping, *Oxid. Met.* **57** (2002), p. 559.

D. Monceau and B. Pieraggi, *Oxid. Met.* **50** (1998), p. 477.

V.K. Tolpygo and D.R. Clarke, *Surf. Coat. Tech.* **120–121** (1999), p. 1.

H.E. Evans, *Mat. High. Temp.* **12** (1994), p. 219.

Corresponding author. Tel.: +33 562885710; fax: +33 562885663.